Effect of ferroelastic twin walls on local polarization switching: Phase-field modeling

S. Choudhury,[1,a)] J. X. Zhang,[1] Y. L. Li,[1] L. Q. Chen,[1] Q. X. Jia,[2] and S. V. Kalinin[3]
[1]*Department of Materials Science and Engineering, Penn State University, University Park, Pennsylvania 16802, USA*
[2]*MPA-STC, MS K763, Los Alamos National Laboratory, Los Alamos, New Mexico 87545, USA*
[3]*The Center for Nanophase Materials Sciences and Materials Sciences and Technology Division, Oak Ridge National Laboratory, Oak Ridge, Tennessee 37831, USA*

(Received 26 February 2008; accepted 10 September 2008; published online 21 October 2008)

Local polarization switching in epitaxial ferroelectric thin films in the presence of ferroelastic domain walls was studied using phase-field approach. The nucleation bias profile across a twin wall was analyzed, and the localization of preferential nucleation sites was established. This analysis was further extended to a realistic domain structure with multiple twin boundaries. It was observed that the local nucleation voltage required for a 180° domain switching is closely related to the number of such local defects. © *2008 American Institute of Physics*. [DOI: 10.1063/1.2993330]

During the past decade, epitaxial ferroelectric thin films have drawn considerable attention for their potential applications in nonvolatile memories[1] and data storage.[2] Progress in these applications necessitates the understanding of polarization switching mechanisms on the nanoscale level of individual capacitor (ferroelectric random access memory) or tip-junction region (data storage), and the role of structural and morphological defects on domain nucleation and wall motion. Following the pioneering work of Landauer[3] it is recognized that ferroelectric domain nucleation in uniform fields is controlled by a number of discrete switching centers, which allows nucleation under a low electric field.[4,5] The role of particular center type in macroscopic switching dynamics is determined by both the center concentration and nucleation activity, i.e., local field required to induce nucleation.

In recent years piezoresponse force microscopy (PFM) has emerged as a powerful technique to study the local switching behavior in ferroelectric materials. In PFM, the inhomogeneous electric field is strongly localized below the tip, resulting in nucleation of domain at the tip-surface junction.[6] Thus PFM offers the possibility of correlating the local switching behavior with the microstructure. The progress in PFM over these years has also stimulated simultaneous development of theoretical models to relate the experimentally observed switching behavior.[7–10] Prior theoretical models typically assume the shape of the nucleated domain as *a priori*, and the thermodynamics of domain switching in PFM was analyzed in a perfect crystal.[3,7,10] Using a combination of the switching spectroscopy PFM and phase-field modeling the authors have shown that in high-quality epitaxial films, the switching bias is close to that expected for intrinsic polarization switching, as can be expected due to the smallness of probed volume and the low defect density.[11] More recently, we developed an approach for mapping local nucleation biases on the ~10 nm level.[12] It was shown that the bias for 180° domain nucleation is lower at the junction of two 90° twin domains compared to the matrix. 90° domain twins (*a*-domains) are known to present in the tetragonal ferroelectric films in the broad range of misfit strains.[13,14] In this manuscript, we present a three-dimensional phase-field model to correlate the switching behavior with the number of twin defects below the tip. As a first example, we present an in-depth analysis of switching behavior with a single defect. We will then study the switching behavior of a realistic domain structure to explain the role of multiple defects.

In phase-field approach, a ferroelectric domain structure is described by the spatial distribution of polarization $\boldsymbol{P}(P_1,P_2,P_3)$. The temporal evolution is described by the time-dependent Ginzburg–Landau equations

$$\frac{\partial P_i(\mathbf{x},t)}{\partial t} = -L\frac{\delta F}{\delta P_i(\mathbf{x},t)}, \quad i=1,2,3, \tag{1}$$

where L is a kinetic coefficient related to the domain wall mobility. F is the total free energy of the system, which includes the bulk free energy F_{bulk}, domain wall energy F_{wall}, elastic energy F_{elas}, and electrostatic energy F_{elec}, i.e.,

$$F = F_{\mathrm{bulk}} + F_{\mathrm{wall}} + F_{\mathrm{elas}} + F_{\mathrm{elec}}. \tag{2}$$

The mathematical expressions for the ferroelectric bulk free energy, ferroelectric domain wall energy, and elastic energy are derived in Ref. 15.

The electrostatic energy of a polarization distribution is

$$F_{\mathrm{elec}} = -\frac{1}{2}\int E_i(\varepsilon_0\kappa_{ij}E_j + P_i)dV, \tag{3}$$

where E_i is the ith component of the electric field related to the electric displacement, D_i, as $D_i=\varepsilon_0\kappa_{ij}E_j+P_i$, where ε_0 is the dielectric permittivity of the vacuum and κ_{ij} is the relative dielectric permittivity of the ferroelectric film. In the absence of space charge, the electrostatic distribution on the film can be obtained from the condition $D_{i,i}=0$, where $D_{i,i}=\partial D_i/\partial x_i$, and the summation convention for the repeated indices is employed. The electrostatic equilibrium equation is solved using a specified boundary condition

[a)]Electronic mail: sxc398@psu.edu.

 © 2008 American Institute of Physics

Downloaded 08 Jan 2009 to 128.118.88.243. Redistribution subject to AIP license or copyright; see http://apl.aip.org/apl/copyright.jsp

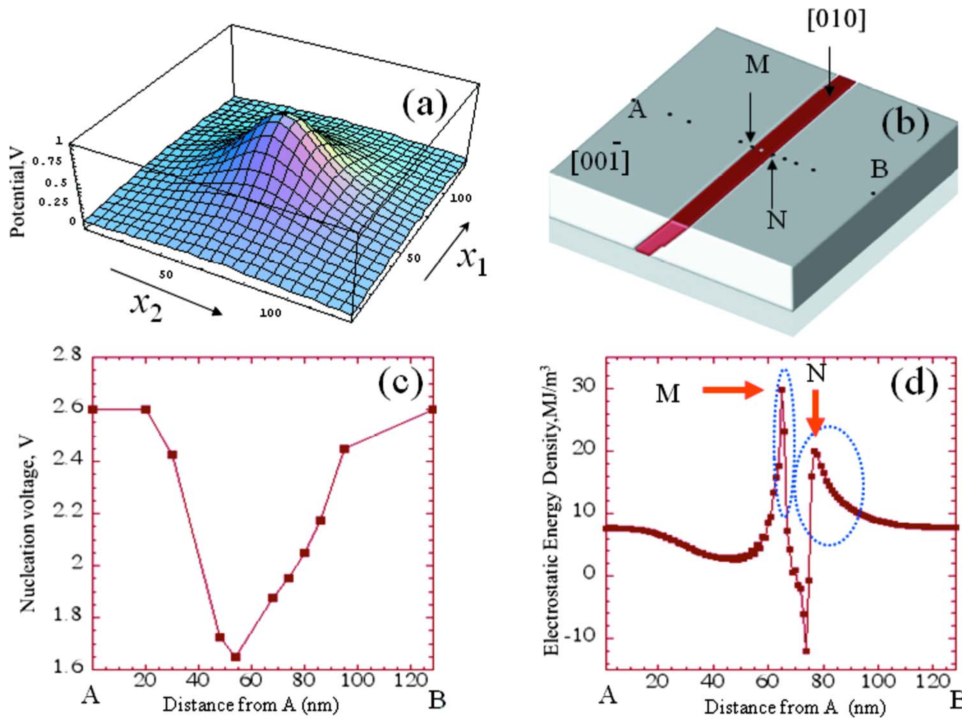

FIG. 1. (Color online) (a) Distribution of the applied potential on the top surface of the thin film for $\{x_1^0, x_2^0\} = \{64, 64\}$; (b) domain structure of epitaxial $PbZr_{0.2}Ti_{0.8}O_3$ thin film with a pre-existing a_2-positive domain within a matrix of c-negative domain under short-circuit boundary condition. The dots show the location of the PFM tip during measurement of nucleation potential along the profile *A-M-N-B*; (c) Spatial distribution of the nucleation potential along the selected profile. Each square symbol indicates the nucleation potential corresponding to a dot in (b); (d) distribution of the electrostatic energy density (MJ/m^3) along the selected profile without any applied potential. Distributions of the electrostatic energy around the two interfaces of the twin domain are marked by the oval shapes.

$$\phi_{\text{substrate-film interface}} = 0, \phi_{\text{film surface}} = \phi_1(x_1, x_2). \tag{4}$$

To model the writing process using the PFM, the tip-induced potential distribution is approximated by a two-dimensional Lorentz-like function

$$\phi_1(x_1, x_2) = \phi_0 \left[\frac{\gamma^2}{(x_1 - x_1^0)^2 + (x_2 - x_2^0)^2 + \gamma^2} \right], \tag{5}$$

where (x_1^0, x_2^0) is the location of the tip (the peak of distribution) and γ stands for the length scale from the tip over which the applied electric potential reduces to half of its peak value. Figure 1(a) shows a typical distribution of the applied potential on the top surface of the thin film. The details on the calculation of electric fields were presented in Ref. 16.

Equation (1) is solved using the semi-implicit Fourier spectral method with periodic boundary conditions in x_1 and x_2 axes along the film plane.[17] The simulation cells were $128\Delta x \times 128\Delta x \times 36\Delta x$ and $256\Delta x \times 256\Delta x \times 36\Delta x$ for the thin films with two domains and multidomains, respectively. The simulation grid spacing is chosen to be $\Delta x = l_0$, where $l_0 = \sqrt{G_{110}/\alpha_0}$ and $\alpha_0 = |\alpha_1|_{T=25\,°C}$. We chose the gradient energy coefficient to be $G_{11}/G_{110} = 0.6$. If $l_0 = 1$ nm, $G_{110} = 1.73 \times 10^{-10}$ $C^{-2}\,m^4\,N$, then the corresponding width of 90° domain wall is about 1.5 nm, which matches well with experimental measurement of domain wall width.[18] Hence, the simulation grid spacing in real space is 1 nm. The thickness of the film is taken as $h_f = 20\Delta x$. The materials parameters are chosen for the epitaxial $PbZr_{0.2}Ti_{0.8}O_3$ thin film.[19] The tip parameter in PFM is chosen as $\gamma = 30$ nm. The average strains induced by the substrate are taken as $\varepsilon_{11} = \varepsilon_{22} = -0.003$. We assumed the domain wall energy to be isotropic. In order to find the critical nucleation potential, we gradually increase the potential ϕ_0 in a step of 0.025 V, and the domain structure from a previous simulation was used as the input at each increment of the potential. At a critical applied electric potential a tetragonal domain with polarization along [001] was found to nucleate below or near the tip and the corresponding electric potential was identified as the nucleation potential.

To examine the role of a single ferroelastic twin boundary, we consider the switching of a film containing an a_2-positive domain within a matrix of c-negative domain [Fig. 1(b)]. The nucleation bias was calculated across the profile *A-M-N-B* as presented in Fig. 1(c). It is clear from the figure that the potential required to nucleate a 180° domain is lower near the twin defect (~1.6 V) as compared to ~2.6 V away from the twin defect within the matrix. The variation of the nucleation voltage around the twin defects reveals that the two interfaces are not equivalent. The potential required to nucleate the 180° domain is lower on the left interface compared to the right interface. Furthermore, the nucleation voltage increases sharply away from the left interface within the matrix compared to the right interface.

To analyze the origins of the asymmetric variation of the nucleation voltage near the two interfaces we map the built-in electrostatic energy density on the surface of the thin film without any applied electric potential [Fig. 1(d)]. The observed asymmetric distribution of the electrostatic energy density can be explained by the interplay between the charge distribution induced by the compressive strain across the domain and depolarization field effect.[12] During switching, the additional energy provides the driving force for 180° domain nucleation, explaining the observed difference of nucleation voltage near the two interfaces. It is noted that electric field ($E_i = -\phi_{,i}$ $i = 1, 2, 3$) exists on the top surface of the thin film due to the applied electric potential gradient along both the out-of-plane direction and the two in-plane directions. The applied electric field displaces the twin wall as the electric potential on the top surface is increased to the nucleation voltage. Thus, the location of the lowest nucleation voltage [Fig. 1(c)] does not exactly corresponds to the locations of the maximum electrostatic energy density [point *M* or *N* in Fig. 1(d)] of the starting domain structure in Fig. 1(b) but

Downloaded 08 Jan 2009 to 128.118.88.243. Redistribution subject to AIP license or copyright; see http://apl.aip.org/apl/copyright.jsp

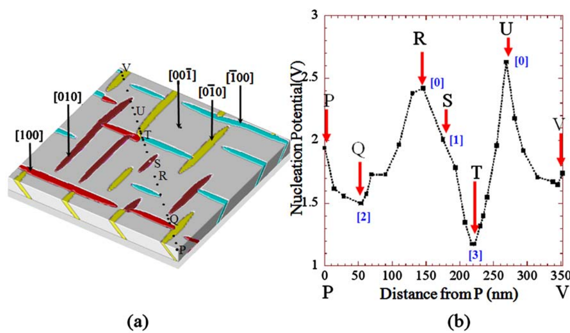

FIG. 2. (Color online) (a) Domain structure of epitaxial $PbZr_{0.2}Ti_{0.8}O_3$ thin film under short-circuit electrostatic boundary condition. Each color represent a tetragonal variant, as indicated; (b) spatial distribution of the nucleation potential along the profile *P-Q-R-S-T-U-V*. Each square symbol indicates the nucleation potential corresponding to a dot in (a). The numbers in the square bracket indicate the number of defects at that particular point. The figure shows the nucleation potential decreases as the number of defect increases.

rather the lowest nucleation voltage is observed at a location within the matrix close to the domain wall. The location of the lowest nucleation voltage corresponds to the position of the twin wall after it is displaced due to the in-plane electric field during the nucleation process. Here, we would also like to point out that the tip parameter γ (30 nm) is broader than the width of the twin domain (~10 nm). Hence, although double maximum in electrostatic energy density exists at each interface of the twin domain, only a single large asymmetric dip in the nucleation voltage near the twin defect is observed instead of two sharp features of nonequal size. Further, it should be pointed out that phase-field simulations show that the voltage required to nucleate 180° domain intrinsically within the matrix is less than 3 V for tip radius of ~30 nm. Thus, on the nearly ideal surface (with no twin defect), the large nonuniform electric field under the PFM tip is sufficient to induce intrinsic polarization switching even for moderately low tip biases.

To understand the spatial distribution of nucleation voltage in a more realistic domain structure in a PZT epitaxial thin film we performed additional phase-field simulations under the short-circuit boundary condition starting from an initial paraelectric state with small random perturbations. The corresponding domain structure is shown in Fig. 2(a). The domain structure consists of a_1 and a_2 twin defects as well as multiple a_1/a_2 domain junctions. To understand the correlation between the spatial variation of nucleation voltage and the domain structure we scanned across the profile *P-Q-R-S-T-U-V* using the probe, and the corresponding variation of the nucleation voltage is presented in Fig. 2(b). It can be seen that the potential to nucleate 180° domain changes continuously across the profile. Furthermore, the figure shows that the nucleation voltage is highest within the matrix (points *R* and *U*) followed by the area around a single twin defect (point *S*), and then by the area where a_1 and a_2 intersects (point *Q*). The lowest nucleation potential is observed near the triple junctions (point *T*). Thus, we conclude that as the number of defects increases the potential required to nucleate a 180° domain decreases.

It should be pointed out that although the predicted nucleation voltage depends on the value of γ chosen during the simulations the spatial distribution of the switching behavior remains unaltered. In addition, we would like to mention that other types of defects such as dislocations and grain boundaries could also affect the spatial distribution of switching behaviors in ferroelectric thin films. Numerical algorithms are now available[20,21] to incorporate such defects and their effect on switching behavior in PFM experiment will be presented in our future publications.

In conclusion, we studied the role of twin defects in ferroelectric thin films on polarization switching under a nonuniform applied electric potential. In the nearly ideal material, the 180° domain can nucleate intrinsically within the matrix. The mechanism of the polarization switching within a single twin defect was analyzed, and observed variability of switching behavior was correlated with built-in electrostatic energy density. Finally, switching of a domain structure with multiple twin defects was studied. It was shown, that the electric potential required for 180° domain switching decreases as the number of twin defects under the tip increases.

We are grateful for the financial supports from NSF under Contract Nos. DMR-0507146 and DMR-0820404 (S.C., J.X.Z., and L.Q.C.) and from the Department of Energy under the Grant No. DOE DE-FG02-07ER46417 (Chen). Research was sponsored in part (S.V.K.) by the Division of Materials Sciences and Engineering, Office of Basic Energy Sciences, U.S. Department of Energy with Oak Ridge National Laboratory, managed and operated by UT-Battelle, LLC. The work at Los Alamos National Laboratory was supported by the U.S. Department of Energy (DOE) through the LANL/LDRD Program.

[1]J. Scott, *Ferroelectric Memories* (Springer, Berlin, 2000).
[2]T. Tybell, C. H. Ahn, and J. M. Triscone, Appl. Phys. Lett. **72**, 1454 (1998).
[3]R. Landauer, J. Appl. Phys. **28**, 227 (1957).
[4]M. E. Lines and A. M. Glass, *Principles and Applications of Ferroelectrics and Related Materials* (Clarendon, Oxford, 1977).
[5]J. F. Scott, J. Phys.: Condens. Matter **18**, R361 (2006).
[6]A. Gruverman, B. J. Rodriguez, C. Dehoff, J. D. Waldrep, A. I. Kingon, R. J. Nemanich, and J. S. Cross, Appl. Phys. Lett. **87**, 082902 (2005).
[7]M. Abplanalp, J. Fousek, and P. Gunter, Phys. Rev. Lett. **86**, 5799 (2001).
[8]M. Molotskii, A. Agronin, P. Urenski, M. Shvebelman, G. Rosenman, and Y. Rosenwaks, Phys. Rev. Lett. **90**, 107601 (2003).
[9]S. V. Kalinin, A. Gruverman, B. J. Rodriguez, J. Shin, A. P. Baddorf, E. Karapetian, and M. Kachanov, J. Appl. Phys. **97**, 074305 (2005).
[10]A. Gruverman, O. Kolosov, J. Hatano, K. Takahashi, and H. Tokumoto, J. Vac. Sci. Technol. B **13**, 1095 (1995).
[11]B. J. Rodriguez, S. V. Kalinin, S. Jesse, Y. H. Chu, T. Zhao, R. Ramesh, S. Choudhury, L. Q. Chen, E. A. Elissev, and A. N. Morozovska, Proc. Natl. Acad. Sci. U.S.A. **104**, 20204 (2007).
[12]S. Jesse, B. J. Rodriguez, S. Choudhury, A. P. Baddorf, I. Vrejoiu, D. Hesse, M. Alexe, E. A. Elissev, A. N. Morozovska, J. X. Zhang, L. Q. Chen, and S. V. Kalinin, Nat. Mater. **7**, 209 (2008).
[13]V. Nagarajan, I. G. Jenkins, S. P. Alpay, H. Li, S. Aggarwal, L. Salamanca-Riba, A. L. Roytburd, and R. Ramesh, J. Appl. Phys. **86**, 595 (1999).
[14]W. Pompe, X. Gong, Z. Suo, and J. S. Speck, J. Appl. Phys. **74**, 6012 (1993).
[15]Y. L. Li, S. Y. Hu, Z. K. Liu, and L. Q. Chen, Acta Mater. **50**, 395 (2002).
[16]Y. L. Li, L. Q. Chen, G. Asayama, D. G. Schlom, M. A. Zurbuchen, and S. K. Streiffer, J. Appl. Phys. **95**, 6332 (2004).
[17]L. Q. Chen and J. Shen, Comput. Phys. Commun. **108**, 147 (1998).
[18]S. Stemmer, S. K. Streiffer, F. Ernst, and M. Ruhle, Philos. Mag. A **71**, 713 (1995).
[19]M. J. Haun, E. Furman, S. J. Jang, and L. E. Cross, Ferroelectrics **99**, 13 (1989).
[20]S. Choudhury, Y. L. Li, C. E. Krill, and L. Q. Chen, Acta Mater. **53**, 5313 (2005).
[21]Y. U. Wang, Y. M. Jin, A. M. Cuitino, and A. G. Khachaturyan, Acta Mater. **49**, 1847 (2001).

Downloaded 08 Jan 2009 to 128.118.88.243. Redistribution subject to AIP license or copyright; see http://apl.aip.org/apl/copyright.jsp